


## Defect Solutions of the Nonreciprocal Cahn-Hilliard Model: Spirals and Targets

Navdeep Rana<sup>1</sup> and Ramin Golestanian<sup>1,2</sup><sup>1</sup>Max Planck Institute for Dynamics and Self-Organization (MPI-DS), D-37077 Göttingen, Germany<sup>2</sup>Rudolf Peierls Centre for Theoretical Physics, University of Oxford, Oxford OX1 3PU, United Kingdom (Received 6 June 2023; revised 16 May 2024; accepted 12 July 2024; published 15 August 2024)

We study the defect solutions of the nonreciprocal Cahn-Hilliard model. We find two kinds of defects, spirals with unit magnitude topological charge, and topologically neutral targets. These defects generate radially outward traveling waves and thus break the parity and time-reversal symmetry. For a given strength of nonreciprocity, spirals and targets with unique asymptotic wave number and amplitude are selected. We use large-scale simulations to show that at low nonreciprocity  $\alpha$ , disordered states evolve into quasistationary spiral networks. With increasing  $\alpha$ , we observe networks composed primarily of targets. Beyond a critical threshold  $\alpha_c$ , a disorder-order transition from defect networks to traveling waves emerges. The transition is marked by a sharp rise in the global polar order.

DOI: 10.1103/PhysRevLett.133.078301

**Introduction**—Constituents of active matter, biological or synthetic, interact in complex ways [1]. These interactions are realized through various mechanisms, for example, chemical activity in colloids and enzymes [2,3], wake-mediated interactions in complex binary plasmas [4], visual perception in bird flocks [5], social communication in crowds of humans [6–8] and microswimmers [9], tensorial hydrodynamic interactions in active carpets [10], and programmable logic in robots [11]. Breaking the action-reaction symmetry leads to novel features that are absent in equilibrium [4,12], including the possibility to engineer multifarious self-organization of building clocks in a choreographed manner [13]. Individuals in a chemically active mixture can assemble into self-propelling small molecules [2,14] or form large cometlike clusters [15,16]. Nonreciprocal alignment interactions lead to a buckling instability of the ordered state in polar flocks [17], as well as a wide range of other novel features [18–20]. In the recently introduced nonreciprocal Cahn-Hilliard model (NRCH) [21–23], parity and time-reversal (PT) symmetries break spontaneously, which leads to the formation of traveling density bands [21,22], coarsening arrest [21,24], and localized states [25]. A variant of the NRCH model with nonlinear nonreciprocal interactions exhibits chaotic steady states where PT symmetry is restored locally in fluctuating domains [23]. Although the NRCH model was introduced phenomenologically [21,22], it has been highlighted

recently that it is possible to derive it as a universal amplitude equation that emerges from a conserved-Hopf instability, occurring in systems with two conservation laws [26]. Moreover, it has been derived using systematic coarse graining of a microscopic model of phoretic active colloids [27].

Here, we study the defect solutions of the NRCH model [21,22]. We find two types of defects, spirals with a unit magnitude topological charge and topologically neutral targets (see Figs. 1 and 2). They are the generators of traveling waves and thus break the PT symmetry. In addition, spirals break the chiral symmetry. Spirals are frequently observed and extensively studied in various systems described by the complex Ginzburg-Landau (CGL) equation, for example, the well-known Belousov-Zhabotinskii reaction, and colonies of *Dictyostelium* [28–32]. Topologically neutral targets are unstable in the framework of the CGL equation but can be stabilized by introducing spatial inhomogeneities [31,33–35]. In the

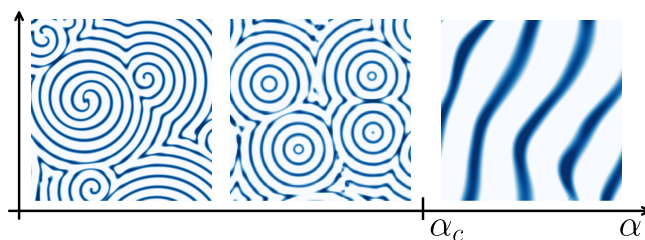


FIG. 1. Qualitative phase portrait for the NRCH model (1) in the  $\alpha$  space. A critical threshold  $\alpha_c$  marks the onset of a disorder-order transition. When nonreciprocal interactions are weak ( $\alpha \ll \alpha_c$ ), we find defect networks with isolated and bound spirals. With increasing  $\alpha$ , targets begin to emerge and are the dominant defects right below  $\alpha_c$ . Above  $\alpha_c$ , noisy global polar order sets in. Fluctuations decay with time, which eventually leads to traveling bands.

Published by the American Physical Society under the terms of the Creative Commons Attribution 4.0 International license. Further distribution of this work must maintain attribution to the author(s) and the published article's title, journal citation, and DOI. Open access publication funded by the Max Planck Society.

context of nonreciprocal interactions, creation and annihilation of spiral defects has been reported in the context of active turbulence in wet polar active carpets [10]. Programmable robots are shown to break the chiral symmetry and spontaneously rotate in clockwise or anti-clockwise manner [11].

*Summary of results*—Our central finding is that the NRCH model admits stable spiral and target defect solutions. Remarkably, no additional spatial inhomogeneities are needed to stabilize the targets [33,34]. For a given strength of nonreciprocal interactions ( $\alpha$ ), defect solutions with a unique asymptotic wave number ( $k_\infty = C\sqrt{\alpha}$ ) and amplitude ( $R_\infty = \sqrt{1 - k_\infty^2}$ ) are selected (see Fig. 2). As a consequence of the wave number selection, defect solutions cease to exist beyond a crossover point  $\alpha_\times = 1/C^2$ . However, in our large-scale numerical simulations starting from disordered states, defect solutions vanish for  $\alpha$  well below  $\alpha_\times$  and we find a disorder-order transition at  $\alpha_c \ll \alpha_\times$  (see Figs. 1 and 3). Below  $\alpha_c$ , an initially disordered state evolves into a quasistationary defect network with no global polar order (see movie 2) in Ref. [36]. While both kinds of defect are stable for a given  $\alpha$ , defect networks exhibit a clear preference for spirals or targets. At small  $\alpha$ , we exclusively find spirals. As we increase  $\alpha$ , targets start to appear as well, and close to the transition point  $\alpha \lesssim \alpha_c$ , we find target-dominated defect networks (see Figs. 3 and 4). Above  $\alpha_c$ , we find traveling waves that show global polar order, rendered imperfect by mesoscopic fluctuations that decay with time and eventually lead to traveling bands. A sharp jump in the global polar order marks the onset of this transition (see Fig. 3).

*Model*—We consider a minimal model of two conserved scalar fields  $\phi_1(\mathbf{r}, t)$  and  $\phi_2(\mathbf{r}, t)$  with nonreciprocal interactions. The complex scalar order parameter  $\phi = \phi_1 + i\phi_2$  obeys the following nondimensional equation [36]

$$\partial_t \phi = \nabla^2 [(-1 + i\alpha)\phi + |\phi|^2 \phi - \nabla^2 \phi], \quad (1)$$

where the parameter  $\alpha$  quantifies the nonreciprocal interactions and  $\alpha > 0$  implies that  $\phi_1$  chases  $\phi_2$ . Conservation of particle numbers for both species makes it impossible to eliminate  $\alpha$  using a global phase transformation as is customarily done for the CGL equation [35]. The length scales of interest are the system size  $L$ , the spinodal instability cutoff length  $\ell$  which for (1) is set to unity, and the length scale  $\ell_\alpha = \ell/\sqrt{\alpha}$  that governs the oscillatory features of (1) [36]. Traveling wave solutions of (1) have the form

$$\phi(\mathbf{r}, t) = R e^{i(k\mathbf{r} - \omega t)}, \quad (2)$$

with  $k = |\mathbf{k}|$ ,  $R = \sqrt{1 - k^2}$ , and  $\omega = \alpha k^2$ . For any  $\alpha$ , an infinite number of plane waves with  $k < 1$  are possible. Waves with  $k < 1/\sqrt{3}$  are linearly stable and small perturbations at wave number  $q$  decay with a rate

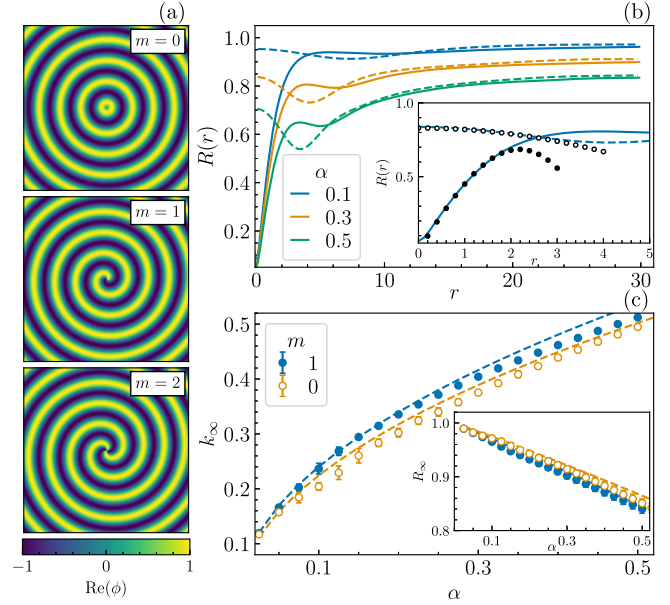


FIG. 2. (a) Defect solutions of the NRCH model. (b)  $R(r)$  vs  $r$  for  $m = 0$  and  $1$  at different  $\alpha \lesssim \alpha_\times$ . Inset: Comparison of  $R(r)$  with small  $r$  approximations [36]. (c) Selected wave number  $k_\infty$  vs  $\alpha$ . We find  $k_\infty = C\sqrt{\alpha}$  (dashed lines with same colours), where  $C \sim 0.76$  for  $m = 1$  and  $C \sim 0.7$  for  $m = 0$ . Inset:  $R_\infty$  vs  $\alpha$  (dashed lines show  $\sqrt{1 - k_\infty^2}$ ).

$\alpha \mathcal{O}(q^2)$ , while beyond this threshold the Eckhaus instability sets in [23,35,38].

*Defect solutions*—We now show that the NRCH model (1) admits defect solutions of the form

$$\phi(\mathbf{r}, t) = R(r) e^{i[m\theta + Z(r) - \omega t]}, \quad (3)$$

where  $r$  and  $\theta$  represent the polar coordinates, and  $r$  is measured from the defect core.  $R(r)$  is the amplitude,  $Z(r)$  is the phase, and  $m$  is the topological charge. Figure 2(a) shows defect solutions for different  $m$ . Topologically neutral target ( $m = 0$ ) and charged spiral ( $m = \pm 1$ ) are stable, whereas defects with  $|m| > 1$  are not and they evolve into a bound pair of spirals. In Fig. 2(b), we plot  $R(r)$  vs  $r$  for various values of  $\alpha$  and  $m$ . An isolated spiral core is singular and stationary, thus  $R(r)$  vanishes at the origin and is independent of time. On the other hand,  $R(r)$  is finite at the core of a topologically neutral target and oscillates slowly with time [28,34,35]. At small  $r$ , we find  $R(r) \sim a_1 r - a_3 r^3$  for spirals and  $R(r) \sim a_0 - a_2 r^2$  for targets. For both spiral and targets, we obtain  $k(r) \equiv (dZ/dr) \sim b_1 r - b_3 r^3$  at small  $r$  [36].

Defects are the generators of plane waves that propagate outwards in the radial direction (see movie 1) [36]. Thus, at large distances from the defect core ( $r \gg 1$ ), the wave front approaches that of a plane wave, i.e.,  $k(r) \rightarrow k_\infty$ , and  $R(r) \rightarrow R_\infty = \sqrt{1 - k_\infty^2}$ . We require  $\omega = \alpha k_\infty^2$  to ensure proper oscillations at all  $r$  and  $k_\infty > 0$  to have a radially

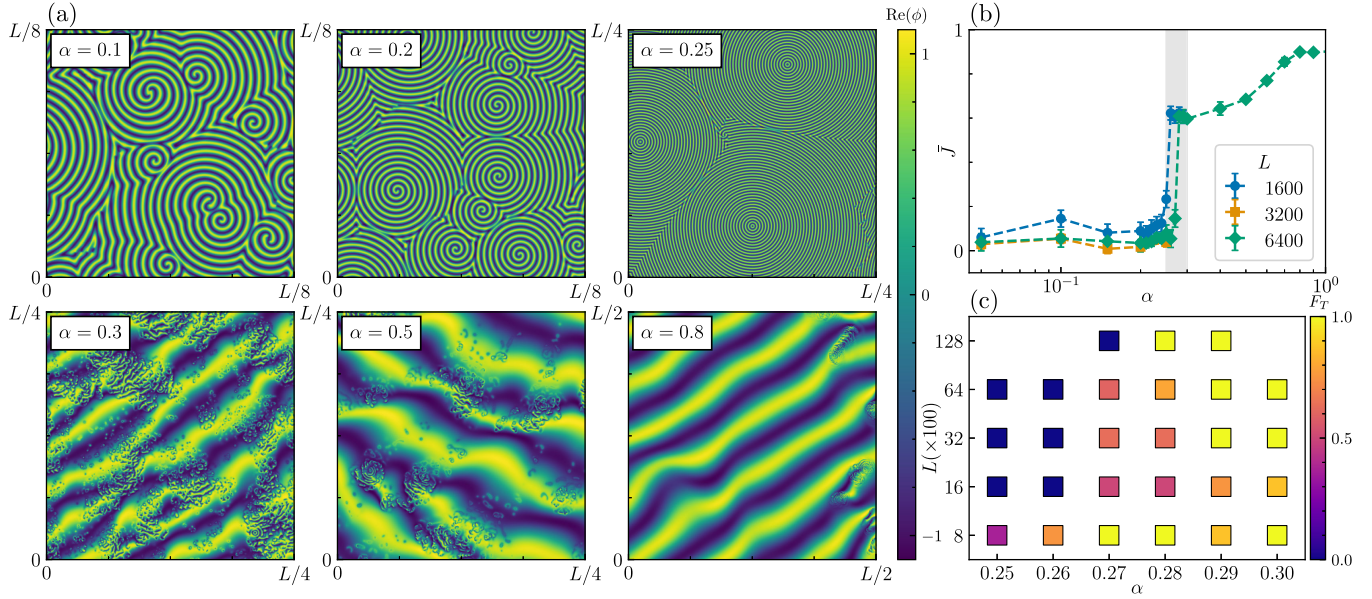


FIG. 3. (a) Transition from disordered defect networks to travelling waves on increasing the nonreciprocity strength  $\alpha$  for  $L = 6400$  and  $N = 4096$  [36]. We plot the real component of  $\phi$  at long times on smaller subdomains for a better visual representation. (b) Global polar order in the steady state with varying  $\alpha$ . At  $\alpha_c$ , we observe a sharp order-disorder transition. (c) Plot of the fraction of simulations ( $F_T$ ) that transition to traveling waves for different  $\alpha$  [shaded region in (b)] and  $L$ . For  $\alpha \geq 0.28$ , almost all of the simulations show the transition and hence we infer  $\alpha_c = 0.28 \pm 0.01$ . Smaller boxes can show transition at  $\alpha \lesssim \alpha_c$  due to finite size effects [36].

outward group velocity, i.e.,  $v_g = 2\alpha k_\infty > 0$  as  $\alpha > 0$ . To first order in  $1/r$ ,  $R(r) \sim R_\infty + (1/r)[(\alpha^2 + k_\infty^4)/2\alpha k_\infty R_\infty]$  and  $k(r) \sim k_\infty + (1/r)(k_\infty^2/2\alpha)$  [36]. Emitted plain waves screen the defect core from outside perturbations [39] and their stability implies that the defect solutions are also stable at large distances from their core. In Fig. 2(c), we show that  $k_\infty$  increases with  $\alpha$  and using a numerical fit we find that  $k_\infty = C\sqrt{\alpha}$ ; the inset verifies the relation between  $R_\infty$  and  $k_\infty$ . It is evident that  $R_\infty$  vanishes for  $\alpha \geq \alpha_x \equiv 1/C^2$  and the defect solutions cease to exist beyond  $\alpha_x$ . Stability of the plane waves then implies a potential crossover from defects to travelling waves for  $\alpha \geq \alpha_x$ . The Eckhaus instability further reduces  $\alpha_x$  as the far field wave fronts are unstable for  $k_\infty > 1/\sqrt{3}$  and we obtain  $\alpha_x = 1/3C^2 \sim 0.58$ .

*Defect networks in simulations*—At equilibrium ( $\alpha = 0$ ), a system quenched from a high temperature disordered state to sub-critical temperatures undergoes bulk phase separation. The phase separated domains grow with time and a unique growing length scale characterizes this coarsening dynamics [40,41]. The dense-dense (liquid-liquid) or dense-dilute (liquid-gas) coexistence states are determined by the reciprocal interactions between the two scalar fields. For  $\alpha \neq 0$ , the interplay of non-reciprocity with equilibrium forces allows for the emergence of *a priori* undetermined complex spatiotemporal patterns; a hallmark feature of nonequilibrium systems [10,42–44]. To understand the dynamical features of the NRCH model, we perform large scale simulations of (1) with varying

nonreciprocity  $\alpha$  and system size  $L$  [36]. In Fig. 3(a), we show the typical steady-state solutions obtained from the evolution of a disordered state. A critical threshold of nonreciprocal interactions,  $\alpha_c < \alpha_x$ , separates the phase space into two distinct regimes—quasistationary defect networks and traveling waves superimposed with local fluctuations [36]. In what follows, we highlight the main features of these nonequilibrium states; a detailed analysis will be presented elsewhere.

For  $\alpha < \alpha_c$  [see Figs. 3(a) (top panels) and 4(a)], after an initial transient period in which numerous newly born defects move around and merge, a quasi stationary steady state emerges (see movie 2, Supplemental Material [36]). This steady configuration is sensitive to the initial conditions and shows limited dynamics. The arms of the isolated spirals rotate, the targets pulsate, and bound pairs of like-charged spirals orbit around a common center. Along the disinclination lines, where the waves emitted from spiral or target cores meet, we find small clusters of additional defects that cannot be classified as spirals or targets. These defects show dynamical rearrangement with time and form locally unsteady patches in an otherwise frozen network (see movie 2) [36]. The composition of defect networks changes with  $\alpha$ . For small  $\alpha$ , we observe isolated spirals and a few bound pairs of like-charged spirals that orbit around a common center. As we increase  $\alpha$ , targets emerge as well and right below  $\alpha_c$ , we primarily find targets. For a given  $\alpha$ , targets show a strikingly higher interdefect separation as compared to the spirals [see Figs. 4(a) and 4(b)]. Because of the sensitivity to the initial

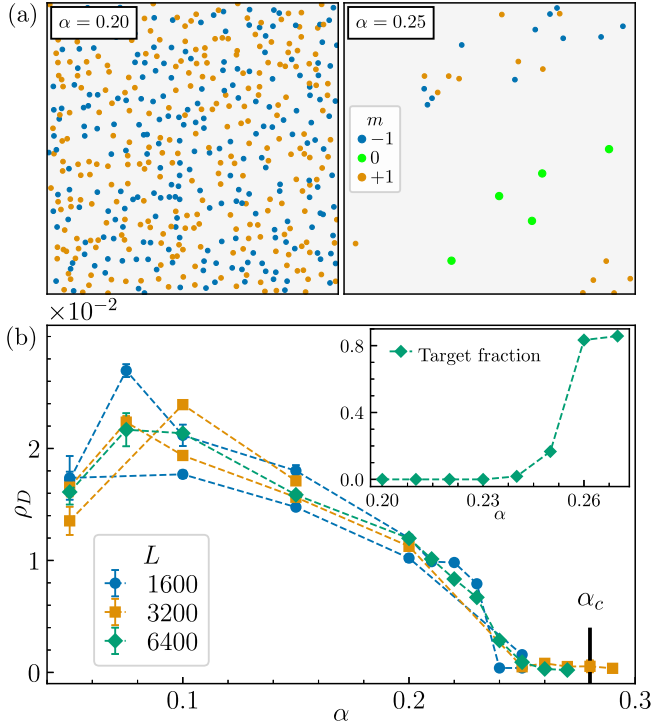


FIG. 4. (a) Scatter plot of spiral and target cores for two different values of  $\alpha$  over the entire simulation domain  $L = 6400$ . Targets show strikingly higher separation compared to spirals. (b) Defect density  $\rho_D$ , defined as the number of spirals and targets per unit area, decreases with increasing  $\alpha$ , in the vicinity of  $\alpha_c$ ,  $\rho_D \sim \mathcal{O}(L^{-2})$  and it vanishes above  $\alpha_c$ . Further, it is sensitive to the initial conditions, as shown by different lines for the same value of  $L$ . Inset: Target fraction increases with  $\alpha$  ( $L = 6400$ ).

conditions, we observe variability in the defect density, but the overall behavior exhibits an initial increase that is then followed by a decrease, as  $\alpha$  is increased [see Fig. 4(b)].

For  $\alpha \gtrsim \alpha_c$ , we find traveling waves [see Fig. 3(a) (bottom panels)]. The transient period shows a mixture of defects and growing patches of polar order, which quickly washes away the defect cores. Afterwards, global polar order, albeit marred by local spatial fluctuations, emerges. These fluctuations decay with time and eventually we find traveling density bands. To quantify the transition from defect networks to traveling waves we compute the average polar order  $\bar{J} \equiv |\langle \hat{J}(\mathbf{r}, t) \rangle|$ , where  $\mathbf{J}(\mathbf{r}, t) \equiv (1/2i)(\phi^* \nabla \phi - \phi \nabla \phi^*) = \phi_1 \nabla \phi_2 - \phi_2 \nabla \phi_1$  is the polar order parameter and  $\langle \dots \rangle$  implies averaging over space and time in the steady state. For a monochromatic plane wave of the form (2),  $\mathbf{J} = R^2 \mathbf{q}$ , and thus  $\bar{J} = 1$ . On the other hand, for defect solutions (3), we have  $\mathbf{J} = R(r)^2(k(r)\hat{r} + (m/r)\hat{\theta})$ , which implies  $\bar{J} \sim 0$ . Far away from the defect cores ( $r \gg \ell$ ), we obtain  $\mathbf{J} \sim R_\infty^2 k_\infty \hat{r}$ , which is independent of the value of  $m$ . The defects emanate radially outward traveling waves and  $\mathbf{J}$  has a topological singularity with unit positive charge at the defect core.

As shown in Fig. 3(b), the transition from defect networks to traveling waves is marked by a sharp increase in the average polar order  $\bar{J}$  at  $\alpha = \alpha_c$ . We find that  $\bar{J} \sim 0$  for defect networks ( $\alpha < \alpha_c$ ), while it acquires a finite value for the traveling wave states  $\alpha > \alpha_c$ . Spatial fluctuations decrease with increasing  $\alpha$ , thus  $\bar{J} < 1$  for  $\alpha \gtrsim \alpha_c$ , while it saturates close to its maximum permissible value  $\bar{J} = 1$  for  $\alpha \gg \alpha_c$ . From Fig. 3(b), we expect  $0.25 < \alpha_c < 0.30$ , however, in the vicinity of  $\alpha_c$ , finite size effects can influence the steady states, especially for smaller box sizes. To obtain a better estimate of  $\alpha_c$ , we have performed an ensemble of numerical simulations with varying box sizes ( $L$ ) spanning 2 orders of magnitude. In Fig. 3(c), we show the fraction of simulations that reached a traveling wave steady state for various  $L$  and  $\alpha$ . From these simulations, we infer  $\alpha_c \sim 0.28 < \alpha_x$ .

*Discussion*—Nonreciprocal interactions emerge naturally in nonequilibrium systems with complex interactions [2,4,45], and this effective breaking of the action-reaction symmetry leads to a variety of novel features. Here, we have unveiled a new feature of nonreciprocal interactions, namely, the emergence of topological defects in binary mixtures of conserved scalar densities. We find two kinds of defects for the NRCH model, spirals with a unit magnitude topological charge and neutral targets. For a given  $\alpha$ , defects with a unique wave number are selected, which immediately predicts a crossover from defects to plain waves at  $\alpha = \alpha_x$ . However, our large-scale numerical simulations show a disorder-order transition from quasistationary defect networks to imperfect global polar order  $\alpha = \alpha_c < \alpha_x$ . These states show a rich phase space behavior. While both charged and neutral defects are allowed for any  $\alpha < \alpha_x$ , at low values of  $\alpha$  the system prefers topologically charged disorder, where the chiral symmetry is broken, and we find isolated and bound pairs of spirals. Close to  $\alpha_c$ , disorder is topologically neutral and targets are the preferred defects. Above  $\alpha_c$ , noisy traveling waves with spontaneously broken polar symmetry emerge. The fluctuations in these states decay with time, but can persist for a very long duration especially for  $\alpha \gtrsim \alpha_c$ .

Our study uncovers important features concerning the phenomenology of active matter with non-reciprocal interactions. We note here that while the isolated defect solutions are stable in the presence of persistent noise, wave interaction and finite size effects can result in interesting pattern formation (see movie 3) [36]. A natural next step will be to study the stability of isolated defect solutions to small perturbations, as has been in the case of the CGL equation [28,35], for which it has been observed that the defect network states are not static but evolve extremely slowly [46]. It will be interesting to investigate if the defect networks in the NRCH model exhibit the phases of vortex liquid and vortex glass with intermittent slow relaxation observed in CGL equation. We have focused here on a simplified version of the NRCH model with

purely nonreciprocal interactions at the linear level and restored global rotational symmetry in the  $\phi$  space [36]. In the Supplemental Material [36] we show the defect solutions in the presence of linear reciprocal interactions. In the future, our study could be extended to the study of the properties of these defect solutions and to include nonlinear nonreciprocal interactions [21]. Finally, in our studies here we have neglected the naturally occurring noise in the NRCH equation, which is conserved and has been found not to affect the stability of long-range polar order in the traveling-bands phase [47]. We note that the existence of noise can help introduce defects in the layered phase, which may (or may not) destabilize the smectic order in the system, as examined in a number of related studies [48–50]. Such considerations will be relegated to future work.

*Acknowledgments*—We thank Giulia Pisegna and Suropriya Saha for fruitful discussions. We acknowledge support from the Max Planck School Matter to Life and the MaxSynBio Consortium which are jointly funded by the Federal Ministry of Education and Research (BMBF) of Germany and the Max Planck Society.

- 
- [1] G. Gompper *et al.*, *J. Phys. Condens. Matter* **32**, 193001 (2020).
- [2] R. Soto and R. Golestanian, *Phys. Rev. Lett.* **112**, 068301 (2014).
- [3] S. Saha, S. Ramaswamy, and R. Golestanian, *New J. Phys.* **21**, 063006 (2019).
- [4] A. V. Ivlev, J. Bartnick, M. Heinen, C.-R. Du, V. Nosenko, and H. Löwen, *Phys. Rev. X* **5**, 011035 (2015).
- [5] M. Ballerini, N. Cabibbo, R. Candelier, A. Cavagna, E. Cisbani, I. Giardina, V. Lecomte, A. Orlandi, G. Parisi, A. Procaccini, M. Viale, and V. Zdravkovic, *Proc. Natl. Acad. Sci. U.S.A.* **105**, 1232 (2008).
- [6] D. Helbing and P. Molnár, *Phys. Rev. E* **51**, 4282 (1995).
- [7] D. Helbing, I. Farkas, and T. Vicsek, *Nature (London)* **407**, 487 (2000).
- [8] K. W. Rio, G. C. Dachner, and W. H. Warren, *Proc. R. Soc. B Biol. Sci.* **285**, 20180611 (2018).
- [9] A. Dinelli, J. O’Byrne, A. Curatolo, Y. Zhao, P. Sollich, and J. Tailleur, *Nat. Commun.* **14**, 7035 (2023).
- [10] N. Uchida and R. Golestanian, *Phys. Rev. Lett.* **104**, 178103 (2010).
- [11] M. Fruchart, R. Hanai, P. B. Littlewood, and V. Vitelli, *Nature (London)* **592**, 363 (2021).
- [12] S. A. M. Loos and S. H. L. Klapp, *New J. Phys.* **22**, 123051 (2020).
- [13] S. Osat and R. Golestanian, *Nat. Nanotechnol.* **18**, 79 (2023).
- [14] R. Soto and R. Golestanian, *Phys. Rev. E* **91**, 052304 (2015).
- [15] J. A. Cohen and R. Golestanian, *Phys. Rev. Lett.* **112**, 068302 (2014).
- [16] J. Agudo-Canalejo and R. Golestanian, *Phys. Rev. Lett.* **123**, 018101 (2019).
- [17] L. P. Dadhichi, J. Kethapelli, R. Chajwa, S. Ramaswamy, and A. Maitra, *Phys. Rev. E* **101**, 052601 (2020).
- [18] R. K. Gupta, R. Kant, H. Soni, A. K. Sood, and S. Ramaswamy, *Phys. Rev. E* **105**, 064602 (2022).
- [19] S. De Karmakar and R. Ganesh, *Phys. Rev. E* **106**, 044607 (2022).
- [20] M. Knežević, T. Welker, and H. Stark, *Sci. Rep.* **12**, 19437 (2022).
- [21] S. Saha, J. Agudo-Canalejo, and R. Golestanian, *Phys. Rev. X* **10**, 041009 (2020).
- [22] Z. You, A. Baskaran, and M. C. Marchetti, *Proc. Natl. Acad. Sci. U.S.A.* **117**, 19767 (2020).
- [23] S. Saha and R. Golestanian, [arXiv:2208.14985](https://arxiv.org/abs/2208.14985).
- [24] T. Frohoff-Hülsmann, J. Wrembel, and U. Thiele, *Phys. Rev. E* **103**, 042602 (2021).
- [25] T. Frohoff-Hülsmann and U. Thiele, *IMA J. Appl. Math.* **86**, 924 (2021).
- [26] T. Frohoff-Hülsmann and U. Thiele, *Phys. Rev. Lett.* **131**, 107201 (2023).
- [27] G. Tucci, R. Golestanian, and S. Saha, *New J. Phys.* **26**, 073006 (2024).
- [28] P. S. Hagan, *SIAM J. Appl. Math.* **42**, 762 (1982).
- [29] A. N. Zaikin and A. M. Zhabotinsky, *Nature (London)* **225**, 535 (1970).
- [30] A. T. Winfree, *Science* **175**, 634 (1972).
- [31] Y. Kuramoto, *Chemical Oscillations, Waves, and Turbulence*, edited by H. Haken, Springer Series in Synergetics Vol. 19 (Springer, Berlin, Heidelberg, 1984).
- [32] K. J. Lee, E. C. Cox, and R. E. Goldstein, *Phys. Rev. Lett.* **76**, 1174 (1996).
- [33] P. S. Hagan, *Adv. Appl. Math.* **2**, 400 (1981).
- [34] M. Hendrey, K. Nam, P. Guzdar, and E. Ott, *Phys. Rev. E* **62**, 7627 (2000).
- [35] I. S. Aranson and L. Kramer, *Rev. Mod. Phys.* **74**, 99 (2002).
- [36] See Supplemental Material at <http://link.aps.org/supplemental/10.1103/PhysRevLett.133.078301>. It includes Ref. [37], for a discussion on the NRCH model and its various solutions, large and small  $r$  behavior of  $R(r)$  and  $k(r)$ , details of the numerical methods, finite-size effects on the defect solutions, and description of the movies.
- [37] S. Cox and P. Matthews, *J. Comput. Phys.* **176**, 430 (2002).
- [38] W. Zimmermann, *Physica (Amsterdam)* **237A**, 405 (1997).
- [39] I. S. Aranson, L. Kramer, and A. Weber, *Phys. Rev. E* **47**, 3231 (1993).
- [40] A. J. Bray, *Adv. Phys.* **51**, 481 (2002).
- [41] A. Onuki, *Phase Transition Dynamics* (Cambridge University Press, Cambridge; New York, 2002).
- [42] M. C. Cross and P. C. Hohenberg, *Rev. Mod. Phys.* **65**, 851 (1993).
- [43] M. C. Marchetti, J. F. Joanny, S. Ramaswamy, T. B. Liverpool, J. Prost, M. Rao, and R. A. Simha, *Rev. Mod. Phys.* **85**, 1143 (2013).
- [44] S. Ramaswamy, *Annu. Rev. Condens. Matter Phys.* **1**, 323 (2010).
- [45] R. Golestanian, in *Active Matter and Nonequilibrium Statistical Physics: Lecture Notes of the Les Houches Summer School: Volume 112, 2018*, edited by J. Tailleur, G. Gompper, M. C. Marchetti, J. M. Yeomans, and C. Salomon (Oxford University Press, New York, 2022).

- [46] C. Brito, I. S. Aranson, and H. Chaté, *Phys. Rev. Lett.* **90**, 068301 (2003).
- [47] G. Pisegna, S. Saha, and R. Golestanian, [arXiv:2404.05396](https://arxiv.org/abs/2404.05396).
- [48] J. Toner and D. R. Nelson, *Phys. Rev. B* **23**, 316 (1981).
- [49] L. Chen and J. Toner, *Phys. Rev. Lett.* **111**, 088701 (2013).
- [50] F. Jülicher, J. Prost, and J. Toner, *Phys. Rev. E* **106**, 054607 (2022).